Membrane-permeabilizing motif in Semliki forest virus E1 glycoprotein

José L. Nieva[a,b,*], Miguel A. Sanz[b], Luis Carrasco[b]

[a] *Unidad de Biofísica (CSIC-UPV/EHU), Departamento de Bioquímica, Universidad del País Vasco, Apdo., 644, 48080 Bilbao, Spain*
[b] *Centro de Biología Molecular (CSIC-UAM), Universidad Autónoma de Madrid, Canto Blanco, 28049 Madrid, Spain*

Received 9 August 2004; revised 15 September 2004; accepted 23 September 2004

Available online 7 October 2004

Edited by Hans-Dieter Klenk

Abstract **Cell infection by alphaviruses is accompanied by membrane permeability changes. New predictive approaches, including the computation of interfacial affinity and corresponding hydrophobic moments, suggest a segmented amphipathic-at-interface domain in the stem region of Semliki Forest virus fusion protein E1. Expression of E1 sequences in *Escherichia coli* cells confirmed that the membrane proximal plus transmembrane (TM) domain unit permeabilizes cells as efficiently as the 6K viroporin. Both our predictive and experimental data support the involvement of the E1 stem-TM region in membrane insertion and permeabilization. We propose to combine Wimley–White hydrophobicity analysis with expression-coupled permeability assays in order to identify viral products implied in breaching cell membrane barriers during infection.**

Keywords: Membrane permeabilization; Membrane fusion; Viral fusion; Semliki Forest virus E1 glycoprotein; Wimley–White hydrophobicity; Hydrophobic moment; Pre-transmembrane

1. Introduction

Alphavirus infection modifies membrane permeability at two well-defined stages, early and late in the lytic cycle [1–4]. Early membrane modifications are provoked by the entry of the virus particles in a process that does not require viral gene expression, since it is the virion glycoproteins that are responsible for early membrane leakiness. Small molecules, as well as proteins, efficiently co-enter with virus particles during the entry of alphaviruses [5,6]. Late modifications lead to an imbalance of ions in the cytoplasm, thus blocking host protein synthesis [3,4,7,8]. The translation of Semliki Forest virus (SFV) subgenomic 26S mRNA is not inhibited by high monovalent ion concentrations, either in vitro or in infected cells [9,10]. Evidence for membrane permeabilization by alphavirus glycoproteins has been obtained by measuring the release of [^{3}H]choline from the interior of liposomes in the presence of virus particles and viral proteins [11]. Complementarily, through electrophysiological measurements, the formation of individual ion-permeable pores at the plasma membrane of cells infected with Sindbis or SFVs can be detected [4,11]. Although not formally proven, there is evidence to suggest that E1 is the glycoprotein with pore-forming capacity in alphaviruses. Pore formation has been detected in proteolytically modified single virions maintaining E1 spike component [12]. Individual expression of alphavirus E1 glycoprotein induces animal cell fusion [13] and pore formation in bacteria [14]. Moreover, its structural homolog, flavivirus E protein, has also been shown to form ion permeable pores [15].

Early results obtained from our laboratory led to the suggestion that the 6K product might be involved in membrane permeabilization at late stages of alphavirus infection. Inducible expression of the 6K gene in *Escherichia coli* cells enhanced membrane permeability to hygromycin B and ^{3}H-choline [16]. Further analysis of 6K interfacial hydrophobicity revealed the presence of two stretches containing invariant Trp residues within the 6K protein ectodomain, exhibiting a high tendency to partition into membrane interfaces [17]. Integration of 6K within the membrane was insufficient for membrane destabilization, the interfacial N-terminal region also being required for membrane permeabilization. A model was proposed according to which a sequence embedded in the membrane interface followed by the transmembrane (TM) anchor represents the minimal structure needed for functional 6K to induce membrane alterations. Again, a similar organization including interfacial helices followed by a TM domain has been described for the stem region of flavivirus E protein [18]. In fact, the structure of mature dengue virus particles determined by cryo-electron microscopy and image reconstruction reveals that the α-helical stem regions of the E molecules are buried in the outer leaflet of the viral membrane [19].

Recently obtained X-ray diffraction data have revealed the three-dimensional structure of SFV E1 glycoprotein lacking the stem-TM regions [20]. Herein, we have used newly developed Wimley–White (WW) scales to analyze hydrophobicity distribution along the crystallographically unsolved SFV E1 elements [21–23]. Our analysis suggests the existence of one segmented membrane-interface associating helix within the stem region, which hypothetically represents a membrane-active site on E1. The inducible expression indicates that the interfacial pre-transmembrane region followed by the TM domain combines to establish a permeabilizing motif at the carboxy terminus of the protein. This region might well participate in the fusion reaction, either as a general destabilizer of bilayer architecture and/or as a creator of a pore-containing bilayer destined for fusion. A similar approach combining prediction with expression-coupled permeability assays

* Corresponding author. Fax: +34-94-601-3360.
E-mail address: gbpniesj@lg.ehu.es (J.L. Nieva).

Abbreviations: IPTG, isopropyl-β-D-thio-galactopyranoside; SFV, Semliki forest virus; TM, transmembrane; WW, Wimley–White

0014-5793/$22.00
doi:10.1016/j.febslet.2004.09.061

might be applied to the analysis of viral genomes in order to identify products and sequences involved in host membrane destabilization.

2. Materials and methods

2.1. Calculating hydrophobic moments

To compute the hydrophobic-at-interface moment, we considered membrane interface-to-water transfer free energies (ΔG_{iwu}) for each amino acid [22,24] as the moduli of the vectors that project from the main axes of the secondary structure element, following the direction of the amino acid side chains [25]. The hydrophobic moment (μ_H) of a sequence of N residues was then calculated as the addition of the N hydrophobicity vectors corresponding to the constituent amino acids, according to the equation [25,26]:

$$\mu_H = \left(\left(\sum_{n=1}^{N} H_n \sin(\delta n) \right)^2 + \left(\sum_{n=1}^{N} H_n \cos(\delta n) \right)^2 \right)^{1/2},$$

where H_n is the hydrophobicity of the n residue and δ is the angle formed between side chains of consecutive residues, i.e., 100° for helical conformations.

2.2. Bacterial expression and permeability changes

DNA manipulations were performed following standard cloning techniques as previously described [16,27]. Briefly, the polymerase chain reaction (PCR) was used to amplify the E1 gene from pGEM1.SFV plasmid (kindly provided by Dr. P. Liljestrom, Karolinska Institute). Oligonucleotides were designed to include codons to stop and initiate translation and to create *Nde*I and *Bam*HI restriction sites. PCR products were purified, analyzed by agarose gel electrophoresis and subsequently ligated with dephosphorylated pET11b vector (kindly provided by B.A. Moffat and F.W. Studier, Brookhaven National Laboratory, NY). The ligation mixtures were used to transform DH5-competent *E. coli* cells. The resulting colonies were screened by digestion with the appropriate restriction enzymes. The region of the plasmids containing the E1 sequences was sequenced by the dideoxy method prior to transforming BL2l(DE3) pLysS *E. coli* cells.

Transformed cells were grown overnight at 37 °C in Luria–Bertani medium in the presence of 100 μg/ml ampicillin and 34 μg/ml chloramphenicol. The cells were then diluted 100-fold in M9 medium supplemented with 0.2% glucose, 2 mM $MgSO_4$, and 0.1 mM $CaCl_2$. Once the cultures reached ca. 0.6 units of absorbance at 660 nm, they were induced by the addition of 1 mM isopropyl-β-D-thio-galactopyranoside (IPTG) (Boehringer Mannheim). 20 min after IPTG addition, the medium was supplemented with 150 μg/ml rifampicin (Boehringer Mannheim) to inhibit transcription by *E. coli* RNA polymerase. Proteins synthesized after culture induction were labeled by placing 1-ml aliquots in tubes containing 1 μCi of [^{35}S]methionine (1.45 Ci/mmol, Amersham Corp.) followed by incubation for 15 min at 37 °C. The labeled bacteria were centrifuged for 1 min at 12 000 rpm in an Eppendorf microcentrifuge and dissolved in lysis buffer (17% glycerol, 0.1 M dithiothreitol, 0.37 M Tris–HC1, pH 6.8, 1% SDS and 0.024% bromphenol blue). The samples were electrophoresed in 0.1% SDS, 20% polyacrylamide gels. Fluorography was conducted by incubation of the gel with 1 M salicylic acid for 1 h. After drying, the gels were exposed to X-ray films at −70 °C.

To determine changes in membrane permeability, two alternative procedures were followed: (1) protein synthesis inhibition by hygromycin B entry and (2) measurement of radioactivity released from [^{3}H]choline or [^{3}H]uridine-preloaded cells. In the first procedure, cells routinely induced for 1 h. were labeled as described with [^{35}S]methionine for 15 min in the presence or the absence of 1 mM hygromycin B (Sigma). Protein production was subsequently analyzed through SDS–PAGE and fluorography. In the second procedure, bacterial cultures grown overnight were diluted in 10–20 ml of M9 medium containing 2 μCi/ml [^{3}H]choline chloride (80 Ci/mmol, Amersham Corp.) or [^{3}H]uridine (60 Ci/mmol, Amersham Corp.) and incubated for 1 h. The cells were then centrifuged for 2 min at 3000 rpm and washed in fresh M9 medium three times. Half of the culture (5–10 ml) was induced as described above. At different times, 200 μl of bacteria was centrifuged at 3000 rpm and the supernatants were mixed with L-929 scintillation mixture (DuPont) to quantify the radioactivity released into the medium.

3. Results and discussion

The upper diagram in Fig. 1 illustrates the structural organization of the E1 protein. An amino-terminal globular β-type structure combines domains I and II, which are followed by immunoglobulin-like domain III. The rest of the sequence including the stem and TM regions is absent from the crystals solved by X-ray diffraction [20]. Hydrophobicity analysis of the unsolved region is shown in the bottom panels. Average hydropathy plots were calculated according to the so-called WW octanol (black) and hydrophobicity-at-interface (gray) scale [28].

The WW octanol scale provides a reasonable estimate of the free energy of inserting α-helical TMDs into bilayers [23,29]. The hydropathy plot displayed in black was computed using octanol-to-water partitioning free energies (ΔG_{ow}), i.e., positive values in the plot denote a tendency to remain in the

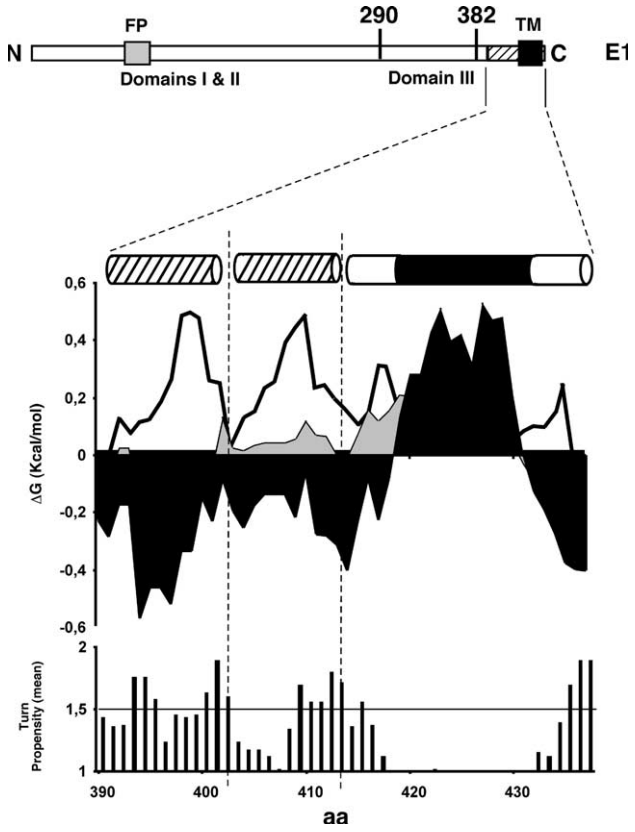

Fig. 1. Hydrophobicity distribution within the E1 stem-transmembrane region. Top: Schematic diagram of SFV E1 showing the location of constituent folding domains and the membrane-interacting FP (fusion peptide) and TM (transmembrane) regions. The WW hydropathy analysis below comprises the stem (hatched box) and TM (black box) regions. Black: TM helix propensity (mean standard free energies of transfer from octanol to water in windows of 11 residues); gray: interfacial hydrophobicity (mean free energies of transfer from membrane interfaces to water in windows of five amino acids); white: average interfacial hydrophobic moment for fixed $\delta = 100°$ and windows of five amino acids. Cylinders on top of the plot indicate the predicted elements: membrane-interface embedded amphipathic helices (hatched) and the TM helical anchor combining interfacial regions (white) with the hydrocarbon core spanning region (black). The bottom plot corresponds to the turn propensity within the stem-TM region. Normalized turn potentials described by Monné et al. [30] for TM sequences were used to calculate average values within sliding windows of five amino acids.

membrane-hydrocarbon mimetic octanol phase. The plot confirms the occurrence of a prominent peak above the 0 equilibrium value (residues 418–432), which would roughly correspond to the membrane anchor spanning the hydrocarbon nucleus as an α-helix. On the other hand, average interfacial hydrophobicity reflects a tendency to remain associated with membrane interfaces. Average membrane interface-to-water partitioning free energy (ΔG_{iw}) values (gray plot) fail to reflect a significant tendency to locate at membrane interfaces within E1 sequences of the stem-TM region. However, computation of the corresponding hydrophobic-at-interface moment for this region reveals the presence of unnoticed membrane-interface associating sequences (white plot). Hydrophobic moments measure the periodicity of residue distribution along secondary structure elements [25,26]. Preferential orientation of the hydrophobic-at-interface residues towards one side of the structure element (amphipathicity-at-interface) is thought to promote the embedding of protein sequences at membrane interfaces [22,24]. The average hydrophobic moment computed using membrane interface-to-water transfer free energies (ΔG_{iwu}) and fixed $\delta = 100°$ detected two main peaks, comprising 10 amino acids each within the pre-transmembrane region. This reflects a tendency to segregate pre-transmembrane residues into defined surfaces of interfacial α-helices. Thus, the particular moment distribution suggests that the E1 preTM might interfacially associate with membranes adopting a segmented amphipathic helical structure. Smaller peaks before and after the octanol peak might represent the boundaries of the TM domain.

In conclusion, the hydrophobicity distribution analysis shown in Fig. 1 suggests the most favorable organization at the stem-TM region of E1 glycoprotein (diagram top) to be: two amphipathic-at-interface α-helices (residues 390–403 and 404–414), preceding a domain that transverses the viral membrane bilayer (residues 415–438), embedded in the external monolayer. Further support for this segmented organization is provided by the distribution within this region of a tendency to adopt interfacial turns (bottom panel) calculated according to the scale described by Monné et al. [30]. The dominance of a turn-inducing tendency (normalized turn potential >1) over a non-inducing one (turn potential <1) is clearly noticeable at positions 400–403 and 412–414.

Based on this prediction, we experimentally characterized the ability of the E1 membrane-proximal region to permeabilize bacterial cells. To this end, we made use of a standard assay developed by our group, in which the Studier system for the expression of toxic proteins in *E. coli* [31–33] is combined with measurements of cell membrane permeability changes coupled to recombinant protein expression [16,34]. Fig. 2 shows cloned E1 sequences (panel A), their expression features (panel B) and their capacity to increase membrane permeability (panel C). In the presence of IPTG and rifampicin, pET11 E1 sequences were the products almost exclusively expressed by cultures. Full E1 protein could be recovered from membrane fractions and its expression resulted moderately toxic as inferred from the decay in protein synthesis with time (panel B). Expression of a single stem-TM domain (E1C) proved to be extremely toxic and could also be detected in association with membrane fractions. Removal of the E1C region to generate E1ecto rendered a product of lower toxicity that could not be detected when associated to membranes.

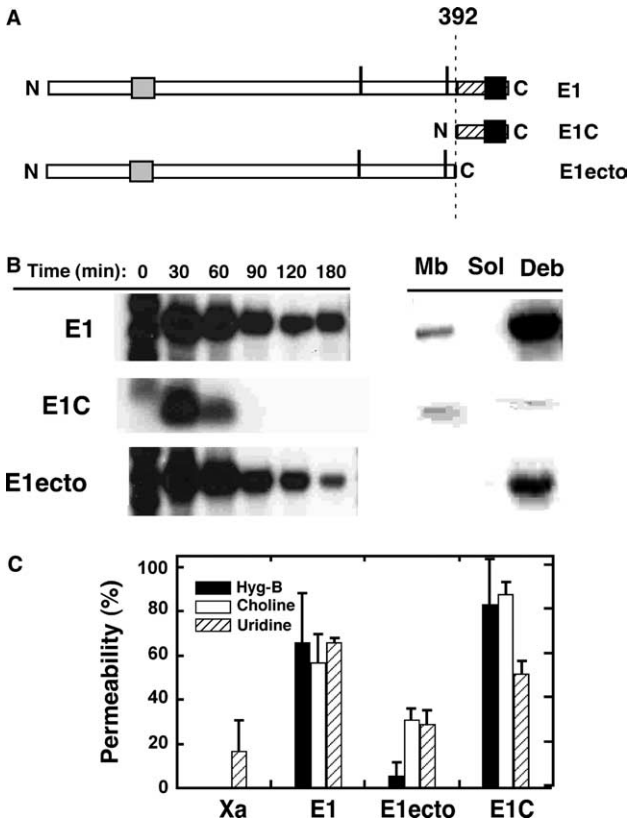

Fig. 2. Expression of E1 sequences in *E. coli* (BL21(DE3) pLysS) and their membrane-permeabilizing activity. (A) Schematic diagrams of expressed E1 sequences. (B) Left panel: fluorographic analysis of SFV E1 proteins synthesized in *E. coli* (BL21(DE3) pLysS strain) from recombinant pET11b plasmids. Bacteria were induced with 1 mM IPTG (time 0) and supplemented with 150 μg/ml rifampicin 20 min after induction. Proteins were labeled at the indicated times with 1 μCi/ml [^{35}S]methionine for 15 min. Right panel: Expression at membranes. The cultures were induced for 60 min, labeled with [^{35}S]methionine and processed for the analysis of membrane fractions: Deb: pellet fraction of cell lysates centrifuged at $10\,000 \times g$ was collected, solubilized with lysis buffer and subjected to SDS–PAGE (see Section 2); Supernatants obtained in the previous centrifugation were subjected to ultracentrifugation at $100\,000 \times g$. Sol: samples collected from supernatant fraction; Mb: idem, but recovered from pellet fraction. (C) Membrane permeabilization according to hygromycin B entry and release of [^{3}H]uridine or [^{3}H]choline. Hygromycin-B entry was estimated through fluorographic analysis from the relative reduction in protein band intensity and area in samples treated with the antibiotic. Expression of XA, a 32-kDa non-toxic protein from phage T7, served as control. Bars represent means of three independent measurements plus standard deviations.

Results shown in panel C are consistent with the involvement of the stem-TM domain in cell permeabilization. This activity can be detected using compounds such as hygromycin B, choline or uridine, as occurs with mammalian cells infected with SFV [2]. The inhibition of protein synthesis by the aminoglycoside antibiotic hygromycin B constitutes a sensitive test for assaying membrane permeability modifications in intact cells [16,34]. The antibiotic did not cross the membrane of induced *E. coli* cells transformed with control non-recombinant pET11b plasmids (not shown) or cells that expressed high levels of recombinant XA protein. Thus, massive protein synthesis or the presence of the expression inducers was insufficient to trigger hygromycin B entry into cells. In contrast, isolated E1 expression allowed hygromycin B entry,

while E1ecto, lacking stem-TM domain, did not. E1C was extremely potent at inducing entry of hygromycin B into cells. Release of compounds from cells preloaded with [^{3}H]choline or [^{3}H]uridine was also maximal for cells expressing the E1C product. Full-length E1-expressing cells showed an intermediate effect, while cells that synthesize E1ecto devoid of stem-TM sequence were less permeable. In conclusion, the capacity to insert into membranes (panel B) and permeabilize them (panel C) seems to specifically locate at the stem-TM E1 region. Of note, E2 expression controls did not alter membrane permeability (data not shown), suggesting that permeabilizing activity may be solely associated to the E1 spike component of SFV.

Experiments depicted in Fig. 3 were designed to demonstrate that E1C-induced permeabilization reflects an intrinsic and specific activity of this product. To this end, a construct encoding SFV E1 TMD (residues 414–438) was generated. Expression of the isolated TME1 product was possible after IPTG/rifampicin induction. Comparable cell lysis was observed upon induction of TME1 and E1C, suggesting that both products inserted into cell membranes and perturbed their integrity (panel A). However, only E1C-expressing cells were permeable to hygromycin B (panel B). Thus, lysis and permeabilization were uncoupled events, the former most likely leading to cell death and protein synthesis abolition, while the latter was specifically determined in the viable cell subpopulation that still performed metabolic functions. Since hygromycin B entry was specifically measured for protein-expressing viable cells, permeabilization must be a direct and specific effect of E1C. The results shown in Fig. 3 also suggest that it is the combination of preTM and TMD sequences that renders the membrane-permeabilizing motif of E1 glycoprotein. This hypothesis is supported by the fact that expression of a product encoding E1 residues 323–417 (i.e., including the preTM region but not the TMD) was not lytic and did not permeabilize cells towards hygromycin B (data not shown).

Interestingly, the TME1 product (25 amino acids) migrated as two bands in SDS–PAGE with apparent molecular weights lower and higher than that of E1C (47 amino acids). The high molecular weight band corresponds to higher order SDS-resistant oligomers. Thus, it is conceivable that membrane oligomerization through this domain might well constitute an important event during the functional E1 cycle.

Finally, we compared membrane activities of the two integral SFV sequences described to contain an interfacial segment preceding the bilayer-spanning domain. In previous work, we proposed this particular membrane topology for 6K based on its hydrophobicity distribution and suggested its involvement in plasma membrane permeabilization during alphavirus infection [17]. The analysis in Fig. 1 and results in Fig. 2 suggest a similar structure-function relationship for E1C. In Fig. 4, we show the kinetics of cell lysis and permeabilization induced by the expression of the E1C moiety and 6K SFV products. In general, induction of both products was lytic for cultures (panel A) and enhanced membrane permeability to uridine (panel B) and choline (panel C). Main differences were noted in uridine release, such that E1C was more active than 6K. This difference was not observed for choline, possibly suggesting slight variations between the permeating structures. Hence, from the results in Fig. 4, it might be inferred that both SFV products have comparable capacities to permeabilize membranes upon their expression.

3.1. Concluding remarks

Two groups of virus-encoded proteins, that interact with membranes, capable of enhancing cell membrane permeability have been described: viral glycoproteins [1,2,35], with a particular architecture in their TM regions and sequences proximal to this domain [21,36]; and viroporins, which include a number of small, very hydrophobic integral membrane proteins [1,23,37]. Despite there being little homology in their primary structure, hydrophobicity distributions along sequences indicate a structural paradigm that might be related to the membrane-activity of some of these proteins, i.e., permeabilizing units consist of integral membrane oligomers composed of membrane-interface residing stretches that are followed by TM anchors. In the case of 6K, we described that interfacial elements, although not required for membrane-association, appear to confer the ability to permeabilize

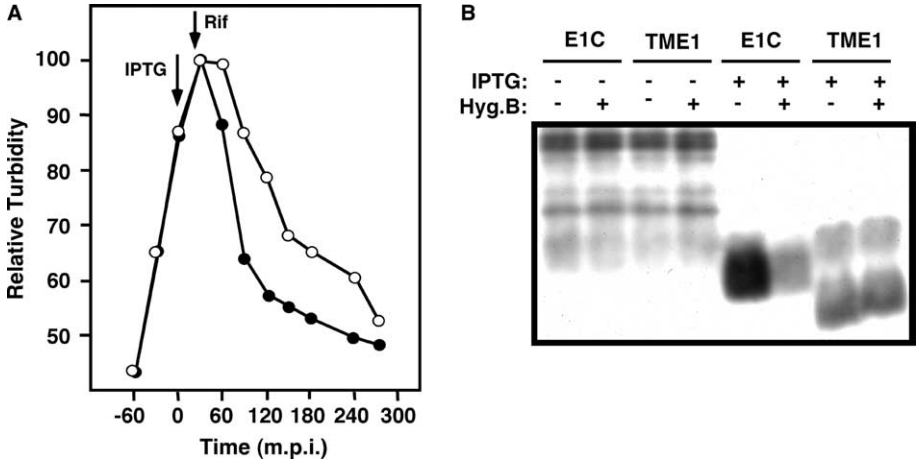

Fig. 3. Comparison of lytic and permeabilizing activities of E1C and TME1 products. (A) Lysis in cultures of induced BL21(DE3) pLysS *E. coli* cells carrying the pET11.TME1 (white symbols) or pET11.E1C (black symbols) constructions. 1-ml culture samples were taken at various times post-induction (arrows) to determine OD at 660 nm. The absorbance measured at 30 min post-induction was taken as 100% value. (B) Protein synthesis and its inhibition by hygromycin B entry.

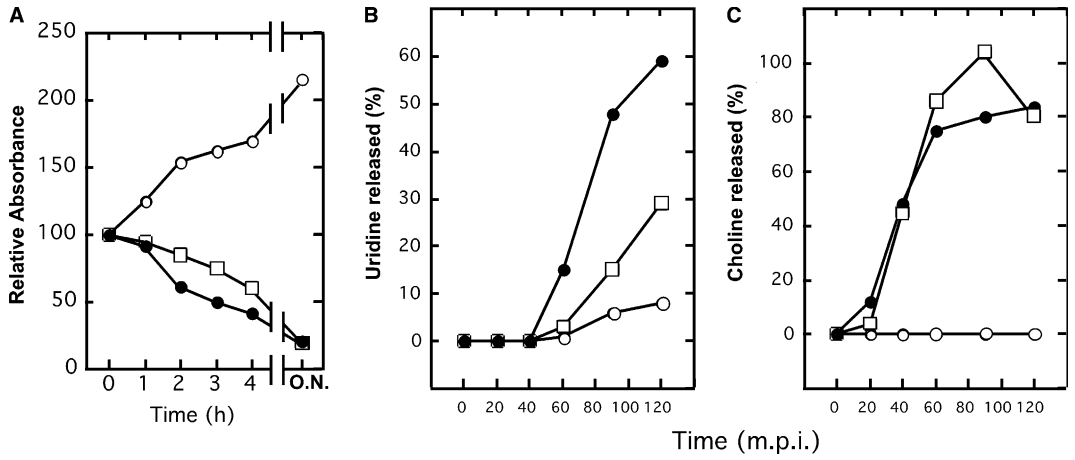

Fig. 4. Comparison of lytic and permeabilizing activities of E1C and 6K products. (A) Lysis in cultures of induced BL21(DE3) pLysS *E. coli* cells carrying the pET11.6K (squares) or pET11.E1C (black circles) constructions. 1-ml culture samples were taken at various times post-induction to determine OD at 660 nm. The absorbance measured at the time of induction was taken as the 100% value. Expression of XA was used as control (white circles). (B) Uridine release upon induction. Cultures of bacteria were pre-loaded with 2 μCi/ml [^{3}H]uridine prior to induction. At different post-induction times, the amount of radioactivity released to the medium was determined. Symbols as for the previous panel. (C) Idem, but cells were preloaded with [^{3}H]choline.

membranes [17]. The present results establish a common trait for the stem-TM region of E1.

We could divide animal viruses into two groups according to the presence or absence of a typical viroporin gene in their genome. Those viruses that code for a viroporin may also contain a glycoprotein with the capacity to alter membrane permeability. Thus, in this case, it may be possible that membrane leakiness at late times of infection is provoked in a redundant manner by two different types of molecules: viroporins and glycoproteins. Another possibility is that glycoproteins only exhibit their permeabilization capacity at early stages of infection, while late permeabilization is mainly provoked by viroporin functioning. In virus species with no evident viroporin gene, other viral molecules might take on their function. For instance, this may be the case for HIV-2 that does not encode the viroporin Vpu, while its TM glycoprotein gp41 is endowed with permeabilizing capacity [22,38]. Other animal viruses, such as Ebola virus, also lack a viroporin gene, but contain glycoproteins that might enhance permeability [24].

In conclusion, our understanding of the molecular basis of membrane permeabilization by viroporins versus viral glycoproteins would benefit much from the identification of motifs that participate in membrane effects. In this regard, the approach presented in this work combining hydrophobicity distribution analysis (prediction) with expression-coupled permeability assays (functional characterization) might become a potent research tool. Nonetheless, it should be noted that this approach relates to membrane-bound equilibrium peptide structures. WW scales constitute a predictive tool because they can be used to identify protein sequences (even those initially folded within globular domains) whose eventual low-energy state is represented by a particular membrane-bound structure [21–24]. Here, we predict that SFV E1 stem-TM sequence in its low-energy configuration adopts a 6K-like permeabilizing membrane structure and expression-coupled permeability assays in bacteria confirm this prediction. Thus, our data constitute a solid starting point for future mutagenesis and structural analyses devoted to elucidate the mechanism of membrane-insertion and subsequent pore-opening within the context of the functional E1 protein.

Acknowledgements: This study was supported by DGICYT Grant BMC2003-00494, CAM Grant 07B/0010/2002 and an institutional grant awarded to the Centro de Biología Molecular "Severo Ochoa" by the Fundación Ramón Areces. Support to J.L.N. includes Grant EET 2001-1954 from Spanish MCyT.

References

[1] Carrasco, L. (1995) Adv. Virus Res. 45, 61–112.
[2] Munoz, A., Castrillo, J.L. and Carrasco, L. (1985) Virology 146, 203–212.
[3] Garry, R.F., Bishop, J.M., Parker, S., Westbrook, K., Lewis, G. and Waite, M.R. (1979) Virology 96, 108–120.
[4] Lanzrein, M., Weingart, R. and Kempf, C. (1993) Virology 193, 296–302.
[5] Fernandez-Puentes, C. and Carrasco, L. (1980) Cell 20, 769–775.
[6] Otero, M.J. and Carrasco, L. (1987) Virology 160, 75–80.
[7] Ulug, E.T., Garry, R.F., Waite, M.R. and Bose Jr, H.R. (1984) Virology 132, 118–130.
[8] Ulug, E.T., Garry, R.F. and Bose Jr., H.R. (1987) in: Mechanism of Viral Toxicity in Animal Cells (Carrasco, L., Ed.), pp. 91–144, Press Inc., Boca Raton, FL.
[9] Alonso, A. and Carrasco, L. (1982) EMBO J. 1, 913–917.
[10] Carrasco, L., Harvey, R., Blanchard, C. and Smith, A.E. (1979) in: Modern Trends in Human Leukemia (Neth, R., Ed.), pp. 227–281, Springer, Berlin.
[11] Wengler, G., Koschinski, A. and Dreyer, F. (2003) J. Gen. Virol. 84, 173–181.
[12] Spyr, C.A., Kaserman, F. and Kempf, C. (1995) FEBS Lett. 375, 134–136.
[13] Sanz, M.A., Rejas, M.T. and Carrasco, L. (2003) Virology 305, 463–472.
[14] Nyfeler, S., Senn, K. and Kempf, C. (2001) J. Biol. Chem. 276, 15453–15457.
[15] Koschinski, A., Wengler, G. and Repp, H. (2003) J. Gen. Virol. 84, 1711–1721.
[16] Sanz, M.A., Perez, L. and Carrasco, L. (1994) J. Biol. Chem. 269, 12106–12110.
[17] Sanz, M.A., Madan, V., Carrasco, L. and Nieva, J.L. (2003) J. Biol. Chem. 278, 2051–2057.

[18] Allison, S.L., Stiasny, K., Stadler, K., Mandl, C.W. and Heinz, F.X. (1999) J. Virol. 73, 5605–5612.
[19] Zhang, W., Chipman, P.R., Corver, J., Johnson, P.R., Zhang, Y., Mukhopadhyay, S., Baker, T.S., Strauss, J.H., Rossmann, M.G. and Kuhn, R.J. (2003) Nature Struct. Biol. 10, 907–912.
[20] Lescar, J., Roussel, A., Wien, M.W., Navaza, J., Fuller, S.D., Wengler, G. and Rey, F.A. (2001) Cell 105, 137–148.
[21] Suárez, T., Gallaher, W.R., Agirre, A., Goñi, F.M. and Nieva, J.L. (2000) J. Virol. 74, 8038–8047.
[22] Sáez-Cirión, A., Gómara, M.J., Lorizate, M., Arrondo, J.L.R., Lloro, I., Melikyan, G. and Nieva, J.L. (2003) Biophys. J. 85, 3769–3780.
[23] Nieva, J.L., Agirre, A., Nir, S. and Carrasco, L. (2003) FEBS Lett. 552, 68–73.
[24] Sáez-Cirión, A., Gómara, M.J., Agirre, A. and Nieva, J.L. (2003) FEBS Lett. 533, 47–53.
[25] Eisenberg, D., Weiss, R.M. and Terwilliger, T.C. (1982) Nature 299, 371–374.
[26] Eisenberg, D., Weiss, R.M. and Terwilliger, T.C. (1984) Proc. Natl. Acad. Sci. USA 81, 140–144.
[27] Sambrook, J., Fritsch, E. R. and Maniatis, T., Eds. (1989) Molecular Cloning: A Laboratory Manual, Cold Spring Harbor Laboratory. Cold Spring Harbor, NY.
[28] Wimley, W. and White, S.H. (1996) Nat. Struct. Biol. 3, 842–848.
[29] White, S.H., Ladokhin, A.S., Jayasinghe, S. and Hristova, K. (2001) J. Biol. Chem. 276, 32395–32398.
[30] Monné, G., Nilsson, I., Elofsson, A. and von Heijne, G. (1999) J. Mol. Biol. 293, 807–814.
[31] Rosenberg, A.H., Lade, B.N., Chui, D.S., Lin, S.W., Dunn, J.J. and Studier, F.W. (1987) Gene 56, 125–135.
[32] Studier, F.W. and Moffatt, B.A. (1986) J. Mol. Biol. 189, 113–130.
[33] Studier, F.W., Rosenberg, A.H., Dunn, J.J. and Dubendorff, J.W. (1990) Methods Enzymol. 185, 60–89.
[34] Lama, J. and Carrasco, L. (1992) J. Biol. Chem. 267, 15932–15937.
[35] Kaserman, F. and Kempf, C. (1996) J. Gen. Virol. 77, 3025–3032.
[36] Garry, R.F. and Dash, S. (2003) Virology 307, 255–265.
[37] Gonzalez, M.E. and Carrasco, L. (2003) FEBS Lett. 552, 28–34.
[38] Arroyo, J., Boceta, M., González, M.E., Michel, M. and Carrasco, L. (1995) J. Virol. 69, 4095–4102.